Real-time monitoring of drug-induced changes in the stomach acidity of living rats using improved pH-sensitive nitroxides and low-field EPR techniques

Dmitrii I. Potapenko [a], Margaret A. Foster [b], David J. Lurie [b], Igor A. Kirilyuk [c],
James M.S. Hutchison [b], Igor A. Grigor'ev [c], Elena G. Bagryanskaya [a],
Valery V. Khramtsov [d,e,*]

[a] *International Tomography Center, Novosibirsk, Russia*
[b] *Biomedical Physics, School of Medical Sciences, University of Aberdeen, Aberdeen AB25 2ZD, UK*
[c] *N.N.Vorozhtsov Novosibirsk Institute of Organic Chemistry, Novosibirsk, Russia*
[d] *Institute of Chemical Kinetics and Combustion, Novosibirsk, Russia*
[e] *Dorothy M. Davis Heart and Lung Research Institute, Division of Pulmonary, Critical Care and Sleep Medicine, the Ohio State University, Columbus, OH 43210, USA*

Abstract

New improved pH-sensitive nitroxides were applied for *in vivo* studies. An increased stability of the probes towards reduction was achieved by the introduction of the bulky ethyl groups in the vicinity of the paramagnetic N—O fragment. In addition, the range of pH sensitivity of the approach was extended by the synthesis of probes with two ionizable groups, and, therefore, with two pK_a values. Stability towards reduction and spectral characteristics of the three new probes were determined *in vitro* using 290 MHz radiofrequency (RF)- and X-band electron paramagnetic resonance (EPR), longitudinally detected EPR (LODEPR), and field-cycled dynamic nuclear polarization (FC-DNP) techniques. The newly synthesized probe, 4-[bis(2-hydroxyethyl)amino]-2-pyridine-4-yl-2,5,5-triethyl-2,5-dihydro-1*H*-imidazol-oxyl, was found to be the most appropriate for the application in the stomach due to both higher stability and convenient pH sensitivity range from pH 1.8 to 6. LODEPR, FC-DNP and proton–electron double resonance imaging (PEDRI) techniques were used to detect the nitroxide localization and acidity in the rat stomach. Improved probe characteristics allowed us to follow *in vivo* the drug-induced perturbation in the stomach acidity and its normalization afterwards during 1 h or longer period of time. The results show the applicability of the techniques for monitoring drug pharmacology and disease in the living animals.
© 2006 Elsevier Inc. All rights reserved.

Keywords: Nitroxide; *In vivo* EPR techniques; *In vivo* pH measurement; Stomach acidity

1. Introduction

Spatially and temporally addressed *in vivo* pH measurements are of considerable clinical relevance. Aberrations of the normal pH homeostasis includes local acidosis induced by ischemia [1,2], infection [3] or inflammation [4], extracellular acidosis in tumors [5], depth-specific tissue pH variations during skin treatments [6] or wound healing [7], etc. Disruption of normal functioning of the gut, such as associated with ulcer formation, or therapeutic intervention of drugs can significantly alter gastric pH [8,9].

Non-invasive pH detection mostly relies on endogenous or/and exogenous molecular probes that are weak acids or bases with pH-dependent spectral properties. Absorption and fluorescent techniques are particularly effective for

---

* Corresponding author. Fax: +1 614 293 4799.
 E-mail address: valery.khramtsov@osumc.edu (V.V. Khramtsov).

pH studies on cellular levels [10,11], while nuclear magnetic resonance, NMR, and electron spin resonance, EPR, have the advantage for *in vivo* applications in animals and humans [12,13]. ^{31}P NMR has been most often used for pH measurement in living tissues based on the pH sensitivity of the chemical shift of endogenous inorganic phosphate, P_i. However pH assessment using ^{31}P NMR and P_i has its own limitations, including lack of resolution (about 0.2–0.3 units and even lower resolution at lower pH), the fact that P_i concentrations vary with metabolism and ischemia, chemical shift dependence on ionic strength, and narrow range of pH measurement near its pK_a value, 6.75 [14–16]. From the above considerations, a number of endogenous and exogenous analogues of phosphates and phosphonates have been tested as alternatives to P_i, among them phosphorus-containing metabolites, such as ATP, 2,3-phosphoglycerate, and glucose 6-phosphate [17–19], and exogenous phosphorus-containing pH probes based on alkyl- and aminophosphonates [20,21]. To increase intrinsic sensitivity of the pH detection by NMR, several exogenous pH probes for ^{19}F NMR [22–24] and ^{1}H NMR [25,26] have been also developed.

A crucial advantage of exogenous EPR probes over NMR is more than three orders of magnitude in sensitivity. However, EPR applications in biological systems are limited by low depth of microwave penetration into aqueous samples. Despite these formidable problems, recently developed low-field EPR-based techniques, such as low-field RF-EPR, LODEPR, FC-DNP offer unique opportunity for non-invasive measurements of the functional EPR probes *in vivo* (for recent reviews see [27,28]). In combination with the steady progress in the design of pH-sensitive nitroxides [29,30] this makes *in vivo* pH detection and imaging possible.

Gallez et al. [31] applied pH-sensitive nitroxide **1** of imidazolidine type and nitroxide **3** of imidazoline type (see Scheme 1) for non-invasive measurement of pH in the stomach of living mice using L-band EPR spectroscopy. Authors demonstrated an ability to detect drug-induced stomach acidity changes. However, the probes **1** ($pK_a = 4.6$) and **3** ($pK_a = 1$) were practically pH-insensitive to the stomach acidity in the most physiologically relevant range from pH 2 to 3.6 due to their inappropriate pK_a values. In our previous work, we demonstrated suitability of LODEPR and FC-DNP for monitoring nitroxide **1** and

measuring pH *in vivo* in rats [27,32]. To extend the accessible range of pH the nitroxide **2** with the $pK_a = 3.0$ was also tested [27]. However hydrophobic character of the probe **2** favoured its membrane localization proved by PEDRI imaging data, and, therefore, compromised its utility to report stomach acidity. The short life time of the probes *in vivo* is another important factor limiting their application. Thus nitroxide **1** showed exponential LODEPR signal decay with characteristic time about 16 min [32]. In this work three improved pH-sensitive nitroxides, namely 3,4-dimethyl-2,2,5,5-tetraethylimidazolidine–1-oxyl, (**4**), 4-dimethylamino-5,5-dimethyl-2-ethyl-2-pyridine-4-yl-2,5-dihydro-1*H*-imidazol-oxyl (**5**) and newly synthesized 4-[bis(2-hydroxyethyl)amino]-2-pyridine-4-yl-2,5,5-triethyl-2,5-dihydro-1*H*-imidazol-oxyl (**6**) were studied (see Scheme 1). To increase stability of the probes towards reduction the bulky ethyl groups in the vicinity of the N─O fragment were introduced. In addition to protonatable nitrogen N-3, a second ionizable group was incorporated into the structure of the probes **5** and **6**, therefore, extending their range of pH sensitivity and the probe hydrophilicity. One of the probes, the nitroxide **6**, was found to be the most appropriate for the pH monitoring in the stomach due to its higher stability, hydrophilic character and convenient pH sensitivity range from pH 1.8 to pH 6. The kinetics of *in vivo* drug-induced perturbation in the stomach acidity in living rats and its normalization afterwards were measured in the physiologically relevant pH range by low-field EPR-based techniques for the first time.

2. Materials and methods

2.1. Chemicals

Diethylenetriaminopentacetic acid (DTPA), sodium and potassium phosphate, NaOH, citric acid, and sodium borate were purchased from Sigma. For measurements of calibration curves buffer containing 50 mM citrate, phosphate, and borate. The synthetic procedures for the nitroxides 3,4-dimethyl-2,2,5,5-tetraethylperhydroimidazol-1-yloxy, **4**, and 5,5-dimethyl-4-(dimethylamino)-2-ethyl-2-pyridine-4-yl-2,5-dihydro-1*H*-imidazol-1-oxyl, **5** (Scheme 1), are described earlier in the references [30,29], respectively. The nitroxide 4-[bis(2-hydroxyethyl)amino]-2-pyridine-4-yl-2,5,5-trimethyl-2,5-dihydro-1*H*-imidazol-oxyl, **6** (Scheme 1),
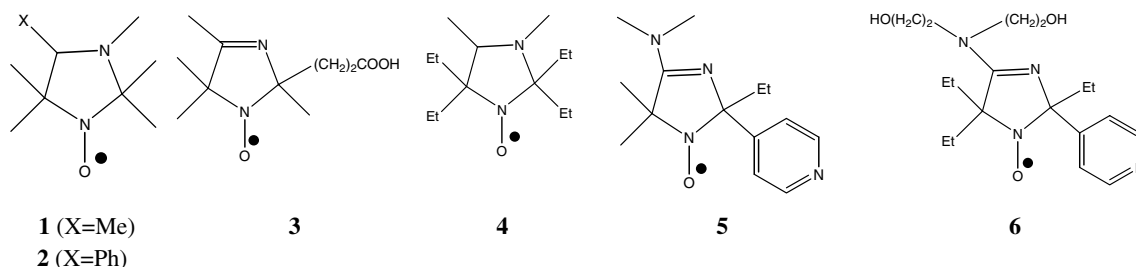
Scheme 1. Structures of the pH-sensitive spin probes **1**–**6**.

was prepared by analogy with the nitroxide **5** [29] as described in Appendix.

2.2. Animals

Thirteen locally bred, male Sprague Dawley rats with weight (BW) 180–200 g were used for *in vivo* studies. The rats were fasted prior to oral intubation (gavage) of 3 ml of 5 mM or 7.5 mM solution of a pH nitroxide label, with or without bicarbonate. Animals were anesthetized by intraperitoneal injection of 41 mg/kg BW ketamine (Vetalar; Parke-Davis, Pontypool, UK) and 20.5 mg/kg BW xylazine (Rompun; Bayer, Bury St. Edmunds, UK), given 1 min after pH label dose. For examination the anesthetized rats were placed in the prone position to aid their respiration and were secured to a plastic support couch that was fitted into the coil assembly of both the LODEPR and the FC-DNP/PEDRI systems. After an examination the animals were killed by pentabarbitone overdose while under anesthesia. All animal procedures were carried out in accordance with local guidelines and under British Home Office project licence no. PPL 60/2309 (M.A.F.).

2.3. X-band EPR measurements

Bruker EMX and Bruker ER-200D-SRC spectrometers were used. The measurements were done in 100 μl quartz tubes. The samples containing buffer solutions of 50 μM nitroxide were titrated to the required pH, placed in the EPR cavity and the spectra were acquired afterwards. Standard spectrometer settings were as follows: microwave power from 1 to 5 mW; number of points, 1024, over sweep width, 80 G (resolution 0.08 G); modulation amplitude, 1 G, for the compounds **5** and **6**, and 3 G for the compound **1** with the broad linewidth; sweep time, 41 s; time constant, 40.96 ms. Hyperfine splitting constant values were determined by fitting of the experimental spectra with WinSim-2000 program package (EPR Spectral Simulation for MS-Windows 9x, NT Version 0.98; Public EPR Software tools; David A. O'Brien, David R. Durling and Dr. Yang C. Fann; National Institute of Environmental Health Sciences; National Institute of Health, USA).

2.4. RF-EPR measurements

A home-made RF-EPR spectrometer was used, operating at 300 MHz [33]. Measurements were carried out on aqueous samples of 1 ml of 0.5–2 mM solution of the radical in glass sample tubes of 10 mm external diameter. Spectra were collected as eight point-by-point averages of 320 point sweeps of a total field 45 G centered on 102.5 G. Sweep time was 32 s or 80.6 s depending on signal intensity. Incident power of 10 mW was applied. Modulation amplitude was 0.5 G at a modulation frequency of 25 kHz. Resonance line positions for nitroxide radical in low magnetic field are given by the Eq. (1) which take into account Breit–Rabi effect [34]. The simplified expressions in

the right part of Eq. (1) were obtained by the substitution of the numerical values for the Planck constant, h, Bohr magneton, μ_B, and nitroxide g-factor, $g = 2.0$ (providing A and H in Gauss, and ω in MHz). Hyperfine splitting values, A, were determined by fitting calculated spectra to the experimental ones using Eq. (1) for the line positions and Lorentzian function for the lineshape.

$$H_{\text{low-field}} = \frac{3A\frac{h}{g\mu_B}\omega - 2\left(\frac{h}{g\mu_B}\omega\right)^2}{A - 2\frac{h}{g\mu_B}\omega} = \frac{3A(\omega/2.79) - 2(\omega/2.79)^2}{A - 2(\omega/2.79)}$$

$$H_{\text{center-field}} = \frac{h\omega}{g\mu_B}\frac{\sqrt{4\left(\frac{h}{g\mu_B}\omega\right)^2 - 9A^2}}{\sqrt{4\left(\frac{h}{g\mu_B}\omega\right)^2 - A^2}} = (\omega/2.79)\frac{\sqrt{4(\omega/2.79)^2 - 9A^2}}{\sqrt{4(\omega/2.79)^2 - A^2}}$$

$$H_{\text{high-field}} = \frac{3A\frac{h}{g\mu_B}\omega + 2\left(\frac{h}{g\mu_B}\omega\right)^2}{A + 2\frac{h}{g\mu_B}\omega} = \frac{3A(\omega/2.79) + 2(\omega/2.79)^2}{A + 2(\omega/2.79)}$$

$$(1)$$

2.5. LODEPR

For this study an in-house-built imager/spectrometer was used in a spectrometer mode [35]. The 50 ml glass or plastic bottle with titrated buffer solution containing 0.5 mM of the radical was placed into magnet bore and spectra were registered. For both *in vitro* and *in vivo* measurements spectra were obtained using an excitation frequency of 304 MHz and a detection frequency of 425 kHz. The field was swept over 45 G centered on 102.5 G with a sweep time of 51.2s or 128 s depending on signal intensity. A time constant of 50 ms was used and normally four averages were taken. The incident RF power level was 5 Ẃ continuous throughout each acquisition period.

2.6. FC-DNP/FC-PEDRI

An in-house-built imager/spectrometer used to collect both FC-DNP spectra and FC-PEDRI images as previously described [36,37]. Images and spectra were collected using field-cycling techniques with an EPR irradiation frequency of 121 MHz applied for 500 ms before each collection of a proton signal, and an NMR frequency of 2.5 MHz. The repetition time (TR) of the pulse sequence was 1200 ms. The average incident power during an acquisition was 8.3 or 16.6 W depending on the study. Spectra were obtained by means of a field-cycled DNP pulse sequence in which the evolution field strength was stepped. The EPR irradiation frequency was maintained constant (as was the NMR frequency), so each step of the evolution field was equivalent to the sampling of an EPR signal at a different magnetic field value [37]. The number of steps and their separation defined the overall width of the observed spectrum and its resolution. In this study, spectra of 60 points over a field range of 55 G centered on 37.5 G (resolution 0.5 G) provided the full three-line spectrum. Spectra

were obtained from living rats or from 150 ml plastic bottles of solutions. The half of the distance between field positions of low and high spectral lines has been used as pH-sensitive spectral parameter. Calculation of the absolute HFS values from FC-DNP spectra was not performed due to low spectral resolution.

Field-cycling PEDRI images were collected as 15x15 cm coronal projective images of the chest and abdomen of the rat with irradiation of the high-field EPR spectral line of the nitroxide at 121 MHz. An interleaved saturation recovery pulse sequence (TR = 1200 ms) with alternate EPR-ON and EPR-OFF was used to collect Overhauser-enhanced and standard NMR images. The difference image obtained by subtraction of the data shows the location of the spin probe in the rat.

2.7. pH titration

Studies of variation in the observed HFS constant, A_{obs}, with pH were made with the use of three low-frequency techniques and by X-band EPR spectroscopy. At X-band three spectral lines are equally spaced and the A_{obs} can be calculated as the distance between neighboring peaks. At low detection frequencies, however, the three lines are unequally spaced due to the Breit–Rabi equation (34). The A_{obs} values were obtained from LODEPR and RF-EPR spectra by fitting the experimental spectra using Lorentzian lineshapes and Eq. (1). For FC-DNP the

observed HFS values were calculated as half the distance between the positions of the high-field and low-field spectral lines. Radical solutions, 50 μM for X-band EPR and 0.5 mM for low-field techniques were prepared in phosphate–citrate buffer (10 mM each). pH was serially adjusted by titration with sodium hydroxide solution or hydrochloric acid to the desired pH with subsequent acquisition of EPR spectra.

3. Results and discussion

3.1. In vitro studies

Scheme 1 shows the structures of the compounds **4**–**6** used in these studies. The compound **4** is tetraethyl-substituted analog of the nitroxide **1** previously used for *in vivo* studies of the stomach acidity [31,32]. Two other nitroxides are three-ethyl substituted nitroxides with an additional bulky group, pyridine, in their structure bound to atom C2 of the radical heterocycle. The introduction of bulky ethyl substitutes in the vicinity of the N—O fragment significantly increases the stability of the nitroxides, as well as prolonging their lifetime in the blood (for the radical **4** and **1** the bimolecular rate constants of the reduction by ascorbate are 0.04 and 0.85 $M^{-1}s^{-1}$, respectively [30]). Typical RF-EPR, LODEPR and FC-DNP spectra of the radicals **4**–**6** are shown in Figs. 1 and 2. Poor solubility of the nitroxide **4** in aqueous solutions and significant broadening
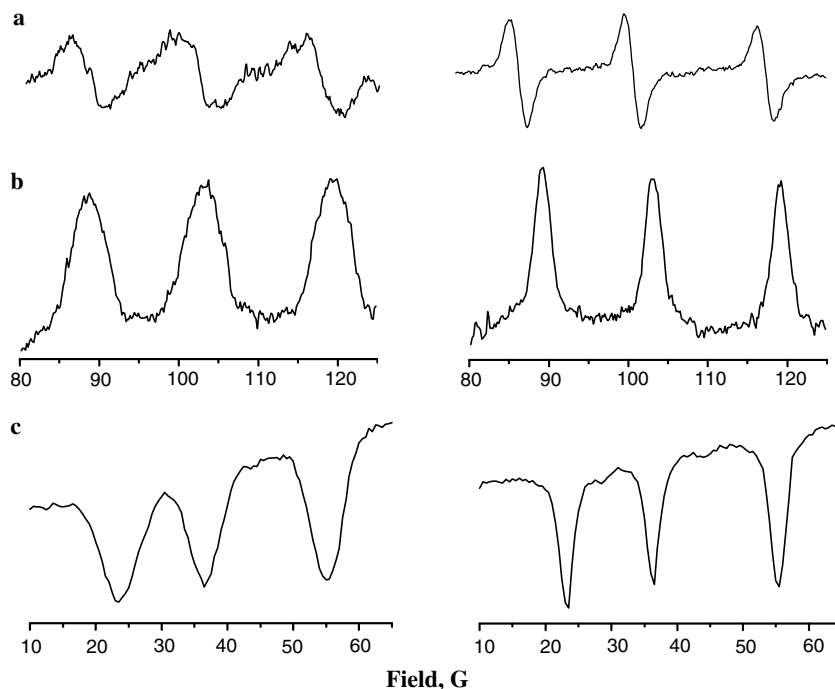

Fig. 1. Low-field spectra of solutions of the nitroxides **4** (left) and **6** (right) in phosphate–citrate buffer (10 mM each) at pH 5.0: (a) RF-EPR spectrum of the samples of 2 ml volume, radical concentration 2 mM, sweep time being equal to 80.6 s; (b) LODEPR spectrum of the samples of 50 ml volume, radical concentration 0.5 mM, sweep time 128 s, RF power 5 W, RF frequency 296 MHz, modulation frequency 193 kHz; (c) FC-DNP spectrum of the sample of 150 ml volume, radical concentration 0.8 mM, sweep time 80.6 s; frequency of EPR irradiation 121.3 MHz. The other spectrometer settings were as described in Section 2.
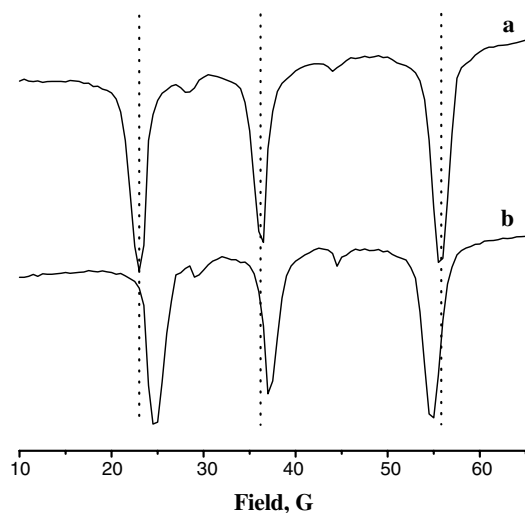
Fig. 2. FC-DNP spectra of the nitroxide **5** obtained in phosphate–citrate buffer (10 mM each) at pH 7 (a) and pH 2 (b). Sample volume was 150 ml. Frequency of EPR irradiation 121.4 MHz. All other settings were as described in Section 2. A dotted line is extended from each peak of the spectra (a) to aid the eye.

Fig. 3. pH Dependencies of the observed HFS constant of the nitroxides **5** (a) and **6** (b). Data were obtained from analysis of FC-DNP ($\triangle$), LODEPR ($\triangledown$), RF-EPR ($\square$) and X-band EPR ($\bigcirc$) spectra as described in Section 2. Solution of the nitroxides in phosphate–citrate buffer (10 mM each) was titrated to necessary pH value and spectra were registered. Sample volumes were 150 ml (nitroxide concentration 0.5 mM), 50 ml (0.5 mM), 2 ml (1 mM) and 150 μl (50 μM) for FC-DNP, LODEPR, RF- and X-band EPR measurements. Solid lines correspond to best fit of obtained data to Eq. (2) yielding parameters A_i and pK_{ai} listed in Table 1.

of its signals compared with the nitroxides **5** and **6** (see Figs. 1 and 2) apparently limit further applications of this probe, particularly *in vivo*, where its membrane localization is expected. Fig. 3 shows the dependencies of the HFS constants of the nitroxides **5** and **6** on pH obtained by X-band and all three low-field EPR techniques. Decrease in pH value of the solution results in reversible decrease of the HFS value.

The titration curves clearly show pH sensitivity of the HFS within extended pH range apparently due to the presence of two ionizable groups with different pK_a values, pK_{a1} and pK_{a2}, in the structure of the nitroxides. The solid lines, shown in Fig. 3, were calculated according to the following equation for the standard titration curve for the compound with two ionizable groups:

$$A_{\text{obs}} = \frac{A_1 + A_2 \times 10^{(\text{pH}-pK_{a1})} + A_3 \times 10^{(2\text{pH}-pK_{a1}-pK_{a2})}}{1 + 10^{(\text{pH}-pK_{a1})} + 10^{(2\text{pH}-pK_{a1}-pK_{a2})}} \quad (2)$$

where A_{obs} is the experimentally measured HFS (see Material and methods); $\text{pH} = -\lg[H^+]$; $A_i(i = 1, 2, 3)$ is the HFS for the nitroxide in the different ionizable forms, namely, neutral, protonated at nitrogen atom N-3, and protonated both at N-3 and pyridine nitrogen atom. Calculated curves are in good agreement with the experimental data with correlation coefficients more than 0.999 for the nitroxides **5** and **6**. Note that the HFS values from RF-EPR and LODEPR spectra, A_{obs}, were calculated taking into account the Breit–Rabi effect (see Section 2) and therefore demonstrates a good agreement with the HFS values obtained from X-band EPR spectra (Fig. 3). Alternatively, a half of the distance between high- and low-field spectral lines can be used to estimate A_{obs} which demonstrates similar pH dependence but yields slightly different absolute HFS values from X-band data particularly for FC-DNP method (see Fig. 3).
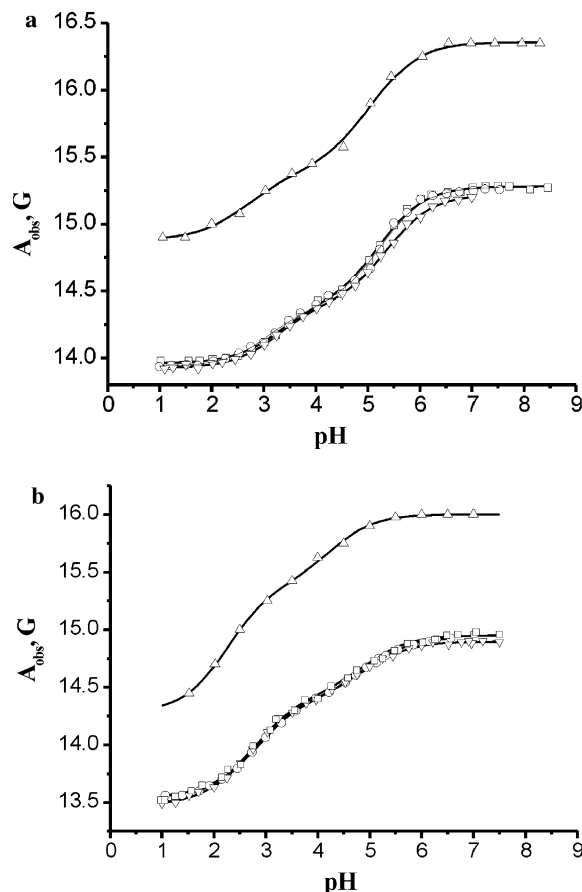
Deviation from high magnetic field approximation most significantly affected the FC-DNP spectra acquired at lowest magnetic field compared with other techniques (cf. field scales for the spectra in Fig. 1). First, small satellite peaks at magnetic field around 29 and 44 G for the nitroxide **5** (Fig. 2) and nitroxide **6** (Fig. 1c, right) were observed. The origin of these peaks is due to the appearance of transitions between electron-nuclear spin levels which are not allowed at higher magnetic fields. Second, the Breit–Rabi effect results in significantly unequal distances between the components of the triplet spectrum (see Eq. (1)). For example, according to (1) for the nitroxide with hypefine splitting, $A = 15$ G, and spectrometer frequency, $\omega = 300$ MHz, the corresponding distances between high-field and central lines and central and low-field lines are 16.15 G and 14.0 G, correspondingly. Table 1 summarizes pK_a and HFS values for the nitroxides **4**–**6** obtained from the fitting of the experimental data to Eq. (2), and pH range accessible to measurement. The nitroxides **5** and **6**

Table 1
pK_a and HFS values for the nitroxides **4**–**6** obtained from fitting the experimental data to Eq. (2), and pH range accessible to measurement by the probe

Nitroxide		X-band EPR	RF-EPR	LODEPR	FC-DNP
4[a]	A_1, G	15.28 ± 0.02	—	15.37 ± 0.07	16.62 ± 0.14
	A_2, G	13.92 ± 0.02	—	13.79 ± 0.01	14.97 ± 0.12
	pK_a	4.96 ± 0.03	—	5.19 ± 0.04	5.10 ± 0.16
	pH range	4–6			
5	A_1, G	15.28 ± 0.01	15.28 ± 0.01	15.22 ± 0.01	16.36 ± 0.04
	A_2, G	14.39 ± 0.02	14.41 ± 0.02	14.41 ± 0.01	15.40 ± 0.05
	A_3, G	13.95 ± 0.01	13.96 ± 0.01	13.93 ± 0.01	14.89 ± 0.05
	pK_{a1}	5.25 ± 0.04	5.23 ± 0.03	5.37 ± 0.02	5.04 ± 0.05
	pK_{a2}	3.09 ± 0.08	3.27 ± 0.07	3.26 ± 0.04	2.69 ± 0.09
	pH range	2.3–6.0			
6	A_1, G	14.93 ± 0.01	14.96 ± 0.01	14.90 ± 0.01	16.03 ± 0.04
	A_2, G	14.40 ± 0.01	14.42 ± 0.02	14.39 ± 0.01	15.67 ± 0.05
	A_3, G	13.54 ± 0.01	13.53 ± 0.01	13.48 ± 0.01	14.50 ± 0.05
	pK_{a1}	4.91 ± 0.03	4.95 ± 0.06	4.87 ± 0.04	4.91 ± 0.05
	pK_{a2}	2.82 ± 0.02	2.73 ± 0.04	2.70 ± 0.02	2.83 ± 0.05
	pH range	1.7–5.8			

[a] An Eq. (2) was applied for fitting HFS dependencies for the nitroxide **4** with a single ionizable group supposing $pK_{a1} = pK_a$ and $pK_{a2} = +\infty$.

have much broader ranges of pH sensitivity compared with the nitroxide **4**, while total pH effects on the HFS value are similar. Normal stomach acidity in rodents varies significantly in the range from pH 2 to 4 depending on the particular animal and the diet [38]. The probe **6** is the most sensitive to pH in this acidity range showing 0.38 G change in the HFS per one pH unit compared with 0.21 G/pH unit for the nitroxide **5** and 0.05 G/pH unit for the nitroxide **3**. Note also that previously used nitroxides **1** and **3** have very low sensitivity to pH in the range of pH from 2 to 4 (0.13 and 0.04 G/pH unit, respectively) [31,32].

3.2. In vivo studies

The nitroxides **5** and **6** with extended spectral pH sensitivity, that covers the stomach acidity, were selected for *in vivo* measurements. Fig. 4 shows LODEPR and FC-DNP spectra from a living rat, which received a 3 ml dose of 5 mM solution of the nitroxide **6** in deionised water by oral intubation. The spectra were registered 11 and 20 min after administration of the dose, respectively, and show good signal to noise ratio (SNR are equal to 20 and 35 for the spectra shown in Figs. 4a and b, correspondingly). The baseline of LODEPR spectra is slightly distorted apparently due to the manganese presented in the rat diet [32]. The FC-DNP spectrum is superimposed on a ramped baseline due to the increase in equilibrium proton magnetization with evolution magnetic field strength. Both techniques provide adequate resolution for accurate determination of line splitting, and hence, of the pH of stomach media.

Typical time dependencies of pH value of stomach media for two rats measured by LODEPR and FC-DNP techniques are shown in Fig. 5. Every rat was administered with 3 ml of gavage contained 5 mM nitroxide **6** alone or together with bicarbonate in deionized water.
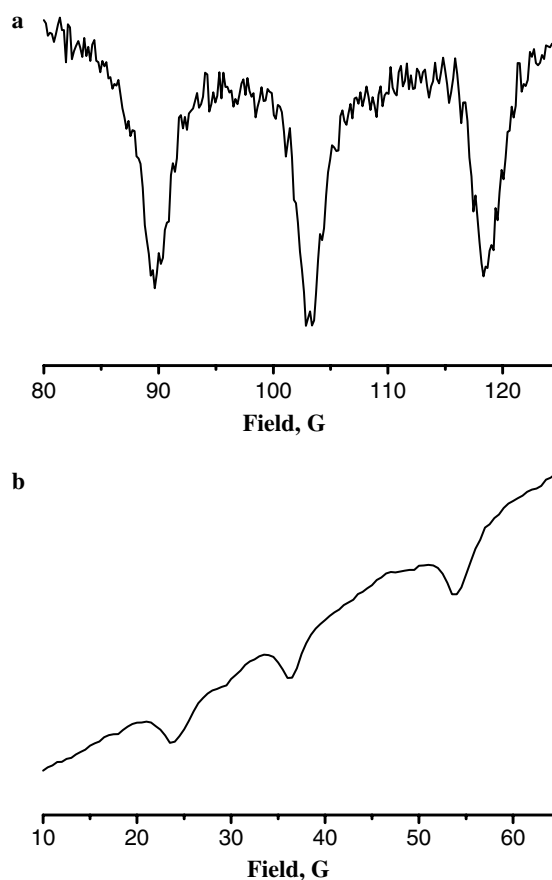

Fig. 4. LODEPR (a) and FC-DNP (b) spectra from a living rat after receiving a 3 ml dose of 5 mM solution of the nitroxide **6**. Spectra were registered 11 min (a) and 20 min (b) after dosing, respectively. Spectrometer settings were as described in Section 2.

Administration of the nitroxide **6** decreases the acidity in the stomach followed by its relaxation to physiological value of pH 2–3 within 20 min. This is not surprising and
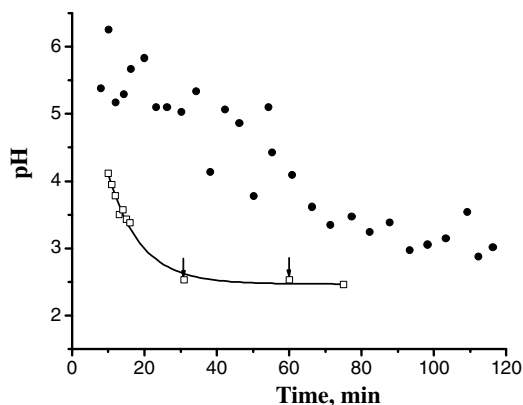
Fig. 5. Time dependencies of pH changes in the stomach measured by LODEPR after giving 3 ml of gavage containing 5 mM nitroxide **6** alone (□) or with 50 mM bicarbonate (●). After dosing the rats were placed in the LODEPR coil assembly and a series of spectra were obtained. In the first case (□) after 15 min the rat was pulled out and placed into the FC-DNP/PEDRI system for subsequent measurements at times marked by arrows. After that the rat was returned to LODEPR coil assembly and one more spectrum was recorded. The sweep time of the LODEPR measurements was 52 s. The frequency of EPR irradiation during FC-DNP spectral acquisition was 121.3 MHz. All other settings were as described in 2. HFS values from each spectrum were determined as described in Section 2 and pH values were calculated from them using data in Fig. 3 as calibration curves. The solid line corresponds to the best fit of the experimental data to exponential function with characteristic time (8.9 ± 1.1) min.

may be explained by the high concentration of the probe, 5 mM, and its weak basic properties with $pK_{a1} = 4.9$ well above of stomach acidity. The absolute values of the changes in pH of the stomach media and characteristic times of its relaxation varied between individual rats, and in most cases allowed fitting to exponential pH relaxation with characteristic time from 5 to 10 min (see Fig. 5 caption). An addition of antacid, bicarbonate, results in a bigger decrease of the initial stomach acidity compared to nitroxide alone, and in much longer relaxation to the physiological value as shown in Fig. 5. Similar *in vivo* kinetics of pH changes were observed upon administration of the nitroxide **5** in the presence or absence of bicarbonate (data not shown). However the data were less reproducible probably due to higher toxicity of the nitroxide **5** (two of six animals given this compound died under anesthesia within half an hour of receiving the gavage).

The observed data demonstrate the ability of the technique to monitor stomach acidity in living animals using nitroxide **6** during the periods of up to 1–2 h over a wide range of pH (Fig. 5). Note that while probe itself perturbs pH in the stomach, its long-life time *in vivo* allows monitoring stomach acidity after pH normalization. In other words the probe really reports the news rather making the news. Fig. 6 shows the decay of intensity of the central line of the LODEPR spectrum for the 5 mM nitroxides **5** and **6** measured *in vivo*. The rate of the decay allows linear interpolation, namely about 50% of the radical intensities are decayed during the first 60 min (nitroxide **6**) or 30 min (nitroxide **5**), still leaving signal intensity enough for regis-
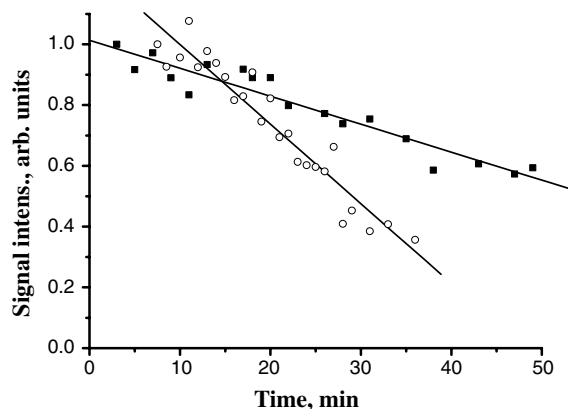

Fig. 6. Time dependencies of signal intensities of the nitroxides **5** (○) and **6** (■) in the rat stomach. The rats received a 3 ml doses containing 5 mM of the nitroxides in deionized water. After administration of a dose animals were placed in the LODEPR coil assembly and the spectra were obtained. Spectrometer settings were as described in Section 2. Signal intensities were measured as the height of the middle line of the recorded spectra.

tration. Note that the rapid *in vivo* decay of the signal intensity of the previously used pH sensitive nitroxide, **1**, with characteristic time of about 16 min [32] was a significant limiting factor in its application (in addition to its low spectral sensitivity to the acidity of solution at pH < 3.6).

Fig. 7 shows a set of FC-PEDRI images of a rat measured 33 min after administration of 3 ml of 5 mM nitroxide **6** in deionized water. It is clearly seen that spin label is localized in the stomach during the time of the experiment, supporting assignment of the previously measured pH values (see Fig. 5) to acidity in the stomach media. The FC-PEDRI images of the distribution of a 5 mM solution of probe **5** measured 23 min after gavage show similar localization of the probe **5** in the animal's stomach (data not shown).

4. Conclusions

Newly synthesized pH-sensitive nitroxides were found to be more stable towards reduction *in vivo* and have extended ranges of pH sensitivity compared with previously available probes. These two factors make these pH probes very useful for *in vivo* real-time monitoring of the stomach acidity. In particular, the nitroxide **6** with two ionizable groups has convenient pH sensitivity range from pH 1.8 to pH 6. The hydrophilic structure of the probe limits its diffusion from the stomach into the membrane compartments while bulky groups in the vicinity to the nitroxyl fragment prevent the radical from reduction. The localization of the nitroxides in the rat stomach was proved by its imaging using PEDRI. The use of the new probes and low-field EPR techniques, LODEPR and FC-DNP, allowed us to follow, for the first time, *in vivo* drug-induced perturbation in the stomach acidity and its subsequent normalization in physiologically relevant pH range over periods of 1 h or longer. The results show the applicability of the approaches
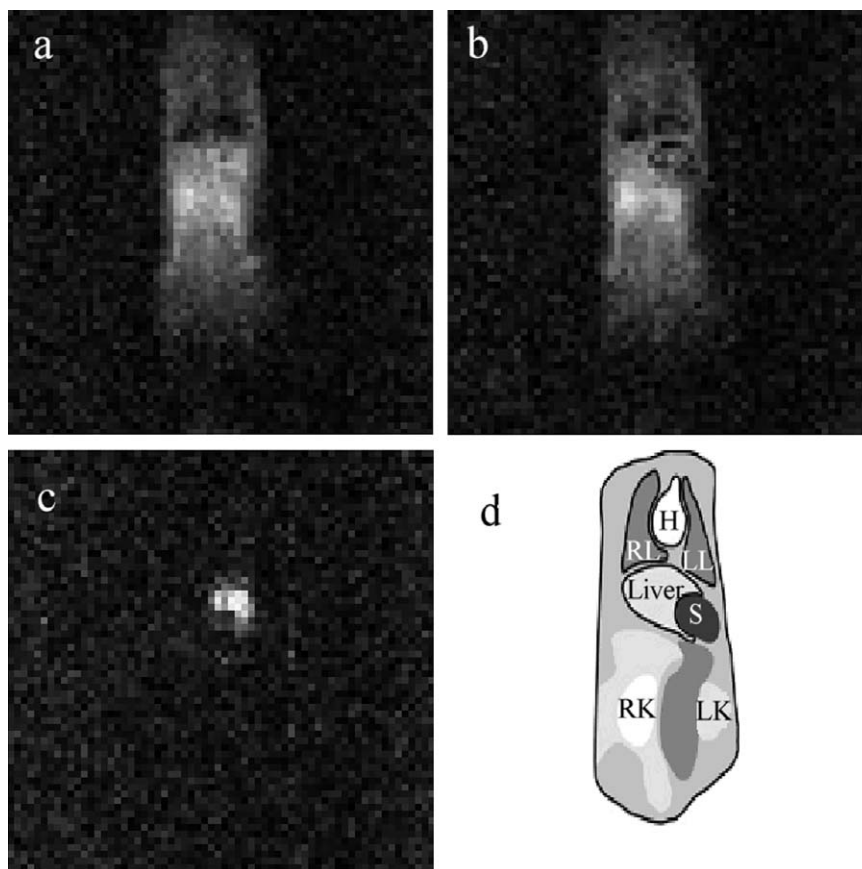
Fig. 7. FC-PEDRI images of a rat gavaged with 3 ml of a 5 mM solutions of nitroxide **6**. Images were taken 33 min after administration of the nitroxide with EPR irradiation off (a), or on (b) and difference between them (c). The diagram (d) demonstrates the anatomy (RL and LL, right and left lungs; H, heart; S, stomach; RK and LK, right and left kidney).

for monitoring drug pharmacology and disease in living animals.

Appendix A. Synthesis of the nitroxide 6

The nitroxide 4-[bis(2-hydroxyethyl)amino]-2-pyridine-4-yl-2,5,5-trimethyl-2,5-dihydro- 1*H*-imidazol-oxyl, **6**, was prepared by analogy with the nitroxide **5** [29] using 3-hydroxyamino-3-ethylpentan-2-one as a starting compound as shown in Scheme 2.

A.1. 5,5-Diethyl-4-methyl-2-pyridine-4-yl-2,5-dihydro-1H-imidazole-1-ol (8)

Pyridine-4-carbaldehyde (2.4 g, 22 mmol) was added to a stirred solution of 3-hydroxyamino-3-ethylpentan-2-one hydrochloride, **7** (4 g, 22 mmol), in ethanol (8 ml) and 25% aqueous ammonia (9 ml). The reaction mixture was stirred for 35 h at 25 °C and allowed to stand at −5 °C overnight. The crystalline precipitate was filtered off, washed with cold 50% EtOH and with cold water, to give dihydroimidazole **8** (3.6 g, 70%) as colorless crystals, mp 132–134 °C (ethyl acetate) (Found: C, 66.85; H, 8.30; N, 18.03. Calcd for $C_{13}H_{19}N_3O$: C, 66.92; H, 8.21; N, 18.01); ν_{max}(KBr)/cm^{-1} 3161, 2966, 2915, 2877, 1643, 1606, 1566, 1482, 1421, 1381, 1312, 1235, 1029, 1003, 893, 872, 830, 786 and 769; λ_{max} (EtOH)/nm 257 (lg ε 3.46); δ_H (400 MHz; CDCl$_3$) 0.77 (3 H, t, J 7.2, CH$_3$, Et), 0.92 (3H, t, J 7.2, CH$_3$, Et), 1.39 and 2.06 (2H each, quartet AB, J_1 7.2, J_2 14.4, 2× CH$_2$, 4-Et), 1.49 (2 H, quartet, J 7.2, CH$_2$, Et), 1.84 (3 H, d, J_2, CH$_3$C=N), 5.43 (1H, quartet, J 2.0, CH), 7.19 and 8.20 (4 H, AA′BB′, J 6.0, Py), 8.35 (1 H, c, OH); δ_C (100 MHz; CDCl$_3$) 8.44, 9.40 (CH$_3$, Et), 25.74, 29.10 (CH$_2$, Et), 16.96 (CH$_3$—C=N), 78.82 (C^5), 92.23 (C^2), 122.46 (C^3, Py), 148.68 (C^2, Py), 150.80 (C^i, Py) and 178.35 (C=N).

A.2. 4,4-Diethyl-5-methyl-2-pyridine-4-yl-4H-imidazole 3-oxide (9)

A suspension of **8** (2.3 g, 10 mmol), and PbO$_2$ (4.78 g, 20 mmol) in CH$_2$Cl$_2$ (30 ml) was stirred for 1–3 h. After the reaction was complete (control by TLC analysis, Silu-
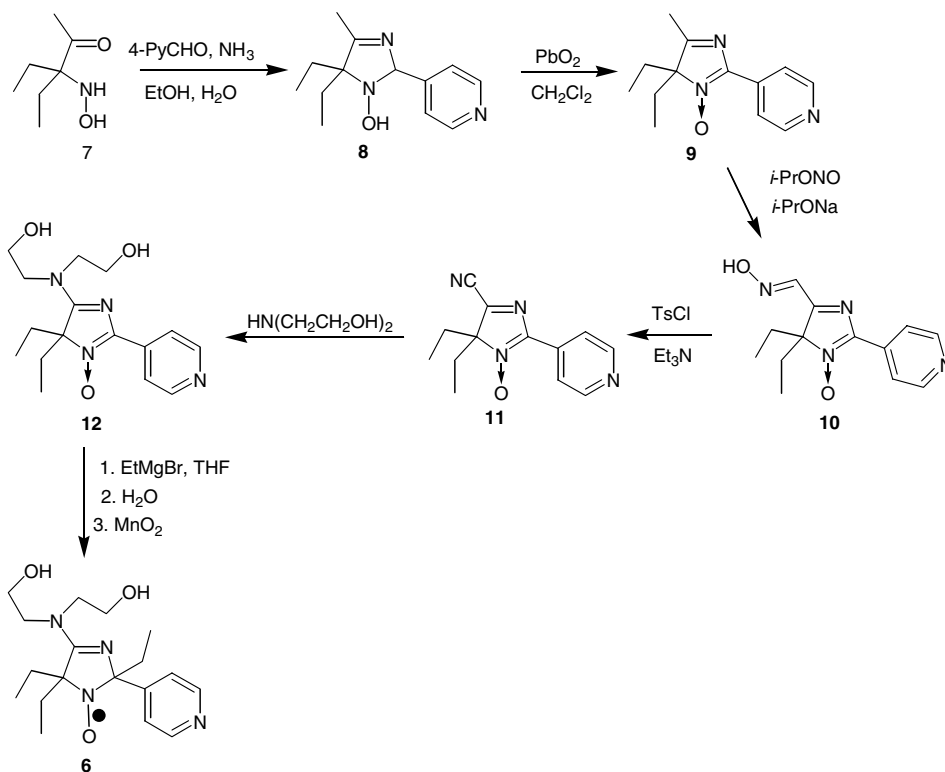
Scheme 2. Synthetic route for the synthesis of the probe **6**.

fol, eluent Et$_2$O–methanol 25:1, development with I$_2$ vapour) the lead oxides were filtered off and the solvent was removed in vacuum to give **9** (2 g 90%) as colorless crystals, mp 81–84 °C (EtOAc–hexane 1:1), (Found: C, 67.29; H, 7.40; N, 18.19; Calcd for C$_{13}$H$_{17}$N$_3$O: C, 67.51; H, 7.41; N, 18.17); ν_{max} (KBr)/cm^{-1} 2973, 2932, 2879, 1595, 1544, 1522, 1477, 1460, 1428, 1403, 1311, 1202, 1060, 991 and 837; λ_{max} (EtOH)/nm 335 (lgε 4.04), 278 (3.81); δ_H (200 MHz; CDCl$_3$) 0.42 (6 H, t, J 7.2, 2 × CH$_3$, 4-Et), 1.69 and 1.94 (2 H each, quartet AB, J$_1$ 7.2, J$_2$ 14.4, 2 × CH$_2$, 4-Et), 2.13 (3H, s, 5-Me), 8.33, 8.61 (2H each, AA′BB′, J 4.8 Hz, Py); δ_C (50 MHz; CDCl$_3$) 6.96 (CH$_3$, Et), 28.53 (CH$_2$, Et), 17.14 (5-Me), 91.28 (C^4), 145.76 (C^2), 178.56 (C^5), Py: 132.97 (C^i), 120.40 (C^3), 150.18 (C^2).

A.3. 4,4-Diethyl-5-methyl-2-pyridine-4-yl-4H-imidazole-5-carbaldehyde oxime (**10**)

Na (1 g, 41 mmol) was dissolved in isopropanol (30 ml); after the reaction became slow the mixture was heated to 60 degrC until Na was completely dissolved. The solution was allowed to cool to room temperature to form a suspension of i-PrONa. Isopropyl nitrite (3.5 ml, 39 mmol) and a solution of **9** (3.7 g, 16 mmol) in 20 ml of isopropanol were added subsequently to the stirred suspension of i-PrONa in isopropanol and the mixture was allowed to stand for 1 h. After the reaction was complete (TLC, Silufol UV-254, eluent EtOAc) the mixture was acidified with AcOH to pH 6 and isopropanol was removed in vacuum. A saturated

solution of NaCl (20 ml) was added to the residue and the precipitate was filtered off and recrystallized from EtOAc to give **10**, (3.3 g, 80%), mp 214–217 (EtOAc), (Found: C, 59.84; H, 6.16; N, 21.60; Calcd for C$_{13}$H$_{16}$N$_4$O$_2$: C, 59.99; H, 6.20; N 21.52); ν_{max} (KBr)/cm^{-1} 1603, 1556, 1523, 1470, 1440, 1409, 1380, 1322, 1206, 1026, 1002, 837, 727 and 706; λ_{max} (EtOH)/nm 359 (lgε 4.02), 256 (4.47); δ_H (400 MHz; ; CDCl$_3$-CD$_3$OD 1:1) 0.57 (6 H, t, J 7.2, 2 × CH$_3$, 4-Et), 2.11 and 2.29 (2 H each, quartet AB, J$_1$ 7.2, J$_2$ 14.4, 2 × CH$_2$, 4-Et), 8.05 (1H, s, HC=N—O), 8.52, 8.71 (2H each, AA′BB′ J 6 Hz, 4-Py); δ_C (50 MHz; CDCl$_3$-CD$_3$OD 1:1) 7.56 (CH$_3$, Et), 31.35 (CH$_2$, Et), 92.90 (C^4), 147.87 (C^2), 171.75 (C^5), 144.29 (HC=NO), Py: 134.12 (C^i), 121.28 (C^3), 150.03 (C^2).

A.4. 4,4-Diethyl-2-pyridine-4-yl-4H-imidazole-5-carbonitrile 3-oxide (**11**)

TsCl (0.95 g, 5 mmol) was added portionwise to a stirred solution of oxime **10** (1.3 g, 5 mmol) of in a mixture of CHCl$_3$ (7.5 ml) and triethylamine (16 ml, 11 mmol). The resulting solution was stirred for 1 h, washed with water and dried over MgSO$_4$. The CHCl$_3$ was removed in vacuum and the residue was separated by column chromatography (Kieselgel 60, Merck, eluent chloroform) to give **11** (0.97 g, 80%), yellow crystals, mp 89–91 (hexane) (Found: C, 64.16; H, 5.76; N, 22.95; Calcd for C$_{13}$H$_{14}$N$_4$O: C, 64.45; H, 5.82; N, 23.13); ν_{max} (KBr)/cm^{-1} 3043, 2974, 2937, 2882, 2220, 1597, 1554, 1508, 1470, 1406, 1409, 1329, 1065, 991, 833, 770 and 710; λ_{max} (EtOH)/nm 372

(lg ε 3.74), 300 (3.95), 239 (4.17), 229 (4.17); δ_H (400 MHz; CDCl$_3$) 0.68 (6 H, t, J 7.6, $2 \times$ CH$_3$, 4-Et), 2.09 and 2.10 (2 H each, quartet AB, J$_1$ 7.6, J$_2$ 14.4, $2 \times$ CH$_2$, 4-Et), 8.31, 8.77 (2H each, AA′BB′ J 6 Hz, 4-Py); δ_C (100 MHz; CDCl$_3$) 7.03 (CH$_3$, Et), 29.17 (CH$_2$, Et), 93.92 (C^4), 111.27 (C$\equiv$N), 147.66 (C^2), 148.36 (C^5), Py: 131.90 (C^i), 119.59 (C^3), 150.61 (C^2).

A.5. 2-[(2-Hydroxyethyl)(4,4-diethyl-2-(4-pyridyl)-3-oxido-4H-imidazol-5-yl)amino]ethanol (12)

2-[(Hydroxyethyl)amino]ethanol (6.5 ml) was triturated with **11** (2.5 g, 10 mmol) and the resulting homogeneous solution was allowed to stand overnight. The reaction mixture was then poured into saturated solution of NaCl (15 ml) and extracted with CHCl$_3$ (3×5 ml). The extract was dried over K$_2$CO$_3$, the CHCl$_3$ was removed in vacuum, and the residue was triturated with Et$_2$O, the precipitate was filtered off to give **12** (1.7 g, 53%), yellow crystals, mp 148–150 °C (THF) (Found: C, 59.71; H, 7.63; N, 17.49. Calcd for C$_{16}$H$_{24}$N$_4$O$_3$: C, 59.98; H, 7.55; N, 17.49); ν_{max} (KBr)/cm^{-1} 2976, 2935, 2861, 1603, 1586, 1558, 1520, 1447, 1428, 1418, 1391, 1312, 1268, 1211, 1176, 1129, 1066, 1052, 1002, 969, 952, 836, 792 and 708; λ_{max} (EtOH)/nm 392 (lg ε 3.69), 267 (4.19); δ_H (200 MHz; CDCl$_3$) 0.68 (6 H, t, J 7.4, $2 \times$ CH$_3$, 4-Et), 1.95 and 2.22 (2 H each, quartet AB, J$_1$ 7.4, J$_2$ 14.4, $2 \times$ CH$_2$, 4-Et), 3.80 (8H, br m, CH$_2$), 4.60 (2H, br s, OH), 8.42, 8.64 (2H each, AA′BB′ J 6 Hz, 4-Py); δ_C (50 MHz; CDCl$_3$) 7.72 (CH$_3$, Et), 28.79 (CH$_2$, Et), 37.99 (N-Me), 52.00 (br, N—CH$_2$), 59.56 (O—CH$_2$), 86.11 (C^4), 146.92 (C^2), 170.14 (C^5), Py: 133.93 (C^i), 121.49 (C^3), 149.81 (C^2).

A.6. 4-[Bis(2-hydroxyethyl)amino]-2-pyridine-4-yl-2,5,5-triethyl-2,5-dihydro- 1H-imidazol-oxyl (6)

One molar of EtMgBr in THF was added dropwise to a stirred solution of **12** (1.6 g, 5 mmol) in THF (10 ml). The reaction was controlled by TLC (Al$_2$O$_3$ Polygram Alox N/ UV 254, Macherey-Nagel, eluent CHCl$_3$–methanol 50:1-2). Usually 3–5 ml of the organometallic reagent solution were sufficient for the reaction to be complete. The reaction mixture was allowed to stand for 0.5 h. The reaction mixture was quenched with water (3 ml). The brown resin precipitate formed was separated from the solution, water (3 ml), Et$_2$O (20 ml), Na$_2$CO$_3$ (1 g) and MnO$_2$ (3 g, 34.5 mmol) were added and the mixture was stirred vigorously for 2 h, the oxidant was filtered off and thoroughly washed with CHCl$_3$–ethanol mixture 1:1. The filtrate was evaporated under reduced pressure, diluted with 1 N NaOH (20 ml) and extracted with t-BuOMe. The extract was dried over Na$_2$CO$_3$. The solvent was removed in vacuum and the nitroxide **6** was isolated from the residue by column chromatography on Al$_2$O$_3$, eluent—t-BuOMe–ethanol 30:1, yield 0.35 g, 20%, yellow crystals, mp 103–105 °C (hexane–t-BuOMe 1:1) (Found: C, 61.87; H, 8.65; N, 15.68. Calcd for C$_{18}$H$_{29}$N$_4$O$_3$: C, 61.87; H, 8.36; N, 16.03); ν_{max} (KBr)/cm^{-1} 2971, 2937, 2876, 1589, 1552, 1466, 1414, 1368, 1327, 1298, 1199, 1138, 1184, 1167, 1066, 1053, 1007, 979, 903, 852, 836 and 810; λ_{max}(EtOH)/nm 222 (lg ε 4.06).

References

[1] J.L. Zweier, P. Wang, A. Samouilov, P. Kuppusamy, Enzyme-independent formation of nitric oxide in biological tissues, Nat. Med. 1 (1995) 804–809.

[2] J.M. Bond, E. Chacon, B. Herman, J.J. Lemasters, Intracellular pH and Ca2+ homeostasis in the pH paradox of reperfusion injury to neonatal rat cardiac myocytes, Am. J. Physiol. 265 (1993) C129–C137.

[3] L.A. Ferrari, L. Giannuzzi, Clinical parameters postmortem analysis and estimation of lethal dose in victims of a massive intoxication with diethylene glycol, Forensic Sci. Int. 153 (2005) 45–51.

[4] U. Issberner, P.W. Reeh, K.H. Steen, Pain due to tissue acidosis: a mechanism for inflammatory and ischemic myalgia? Neurosci. Lett. 208 (1996) 191–194.

[5] N. Raghunand, R.J. Gillies, pH and drug resistance in tumors, Drug. Resist. Updat. 3 (2000) 39–47.

[6] C. Kroll, W. Hermann, R. Stosser, H.H. Borchert, K. Mäder, Influence of drug treatment on the microacidity in rat and human skin—an *in vitro* electron spin resonance imaging study, Pharm. Res. 18 (2001) 525–530.

[7] B. Greener, A.A. Hughes, N.P. Bannister, J. Douglass, Proteases and pH in chronic wounds, J. Wound Care 14 (2005) 59–61.

[8] T. Fukuchi, K. Ashida, H. Yamashita, N. Kiyota, R. Tsukamoto, H. Takahashi, D. Ito, R. Nagamatsu, Influence of cure of *Helicobacter pylori* infection on gastric acidity and gastroesophageal reflux: study by 24-h pH monitoring in patients with gastric or duodenal ulcer, J. Gastroenterol. 40 (2005) 350–360.

[9] R. Zhou, P. Moench, C. Heran, X. Lu, N. Mathias, T.N. Faria, D.A. Wall, M.A. Hussain, R.L. Smith, D. Sun, pH-dependent dissolution *in vitro* and absorption *in vivo* of weakly basic drugs: development of a canine model, Pharm. Res. 22 (2005) 188–192.

[10] R.G. Zhang, S.G. Kelsen, J.C. LaManna, Measurement of intracellular pH in hamster diaphragm by absorption spectrophotometry, J. Appl. Physiol. 68 (1990) 1101–1106.

[11] A. Molich, N. Heisler, Determination of pH by microfluorometry: intracellular and interstitial pH regulation in developing early-stage fish embryos (*Danio rerio*), J. Exp. Biol. 208 (2005) 4137–4149.

[12] R.J. Gillies, N. Raghunand, M.L. Garcia-Martin, R.A. Gatenby, pH imaging. A review of pH measurement methods and applications in cancers, IEEE Eng. Med. Biol. Mag. 23 (2004) 57–64.

[13] V.V. Khramtsov, Biological imaging and spectroscopy of pH, Curr. Org. Chem. 9 (2005) 909–923.

[14] R.J. Gillies, J.R. Alger, J.A. den Hollander, R.G. Shulman, Intracellular pH measured by NMR: methods and results, in: R. Nuccitelli, D.W. Deamer (Eds.), Intracellular pH: Its Measurement, Regulation and Utilization in Cellular Functions, Alan R. Liss, New York, 1992, pp. 79–104.

[15] S. Martel, J.L. Clement, A. Muller, M. Culcasi, S. Pietri, Synthesis and ^{31}P NMR characterization of new low toxic highly sensitive pH probes designed for *in vivo* acidic pH studies, Bioorg. Med. Chem. 10 (2002) 1451–1458.

[16] A.S. Ojugo, P.M. McSheehy, D.J. McIntyre, C. McCoy, M. Stubbs, M.O. Leach, I.R. Judson, J.R. Griffiths, Measurement of the extracellular pH of solid tumours in mice by magnetic resonance spectroscopy: a comparison of exogenous (19)F and (31)P probes, NMR Biomed. 12 (1999) 495–504.

[17] P.M.L. Robitaille, P.A. Robitaille, G.G. Brown, An analysis of the pH-dependent chemical-shift behavior of phosphorus-containing metabolites, J. Magn. Reson. 92 (1991) 73–84.

[18] G.D. Williams, T.J. Mosher, M.B. Smith, Simultaneous determination of intracellular magnesium and pH from the three ^{31}P NMR chemical shifts of ATP, Anal. Biochem. 214 (1993) 458–467.

[19] L.H. Schliselfeld, C.T. Burt, R.J. Labotka, ^{31}P nuclear magnetic resonance of phosphonic acid analogues of adenosine nucleotides as functions of pH and magnesium ion concentration, Biochemistry 21 (1982) 317–320.

[20] K. Bruynseels, N. Gillis, P. Van Hecke, F. Vanstapel, Phosphonates as ^{31}P-NMR markers of extra- and intracellular space and pH in perfused rat liver, NMR Biomed. 10 (1997) 263–270.

[21] S. Pietri, M. Miollan, S. Martel, F. Le Moigne, B. Blaive, M. Culcasi, alpha- and beta-phosphorylated amines and pyrrolidines, a new class of low toxic highly sensitive ^{31}P NMR pH indicators. Modeling of pK_a and chemical shift values as a function of substituents, J. Biol. Chem. 275 (2000) 19505–19512.

[22] C. Deutsch, J.S. Taylor, M. Price, pH homeostasis in human lymphocytes: modulation by ions and mitogen, J. Cell. Biol. 98 (1984) 885–893.

[23] S. He, R.P. Mason, S. Hunjan, V.D. Mehta, V. Arora, R. Katipally, P.V. Kulkarni, P.P. Antich, Development of novel ^{19}F NMR pH indicators: synthesis and evaluation of a series of fluorinated vitamin B6 analogues, Bioorg. Med. Chem. 6 (1998) 1631–1639.

[24] Y. Aoki, K. Akagi, Y. Tanaka, J. Kawai, M. Takahashi, Measurement of intratumor pH by pH indicator used in ^{19}F-magnetic resonance spectroscopy. Measurement of extracellular pH decrease caused by hyperthermia combined with hydralazine, Invest. Radiol. 31 (1996) 680–689.

[25] M.S. Gil, Imidazol-1-ylalkanoate esters and their corresponding acids. A novel series of extrinsic ^{1}H NMR probes for intracellular pH, Bioorg. Med. Chem. Lett. 2 (1992) 1717–1722.

[26] R. van Sluis, Z.M. Bhujwalla, N. Raghunand, P. Ballesteros, J. Alvarez, S. Cerdan, J.P. Galons, R.J. Gillies, *In vivo* imaging of extracellular pH using ^{1}H MRSI, Magn. Reson. Med. 41 (1999) 743–750.

[27] V.V. Khramtsov, I.A. Grigor'ev, M.A. Foster, D.J. Lurie, I. Nicholson, Biological applications of spin pH probes, Cell. Mol. Biol. 46 (2000) 1361–1374.

[28] V.V. Khramtsov, I.A. Grigor'ev, M.A. Foster, D.J. Lurie, *In vitro* and *in vivo* measurement of pH and thiols by EPR-based techniques, Antioxid. Redox Signal. 6 (2004) 667–676.

[29] I.A. Kirilyuk, A.A. Bobko, V.V. Khramtsov, I.A. Grigor'ev, Nitroxides with two pK values—useful spin probes for pH monitoring within a broad range, Org. Biomol. Chem. 3 (2005) 1269–1274.

[30] I.A. Kirilyuk, A.A. Bobko, I.A. Grigor'ev, V.V. Khramtsov, Synthesis of the tetraethyl substituted pH-sensitive nitroxides of imidazole series with enhanced stability towards reduction, Org. Biomol. Chem. 2 (2004) 1025–1030.

[31] B. Gallez, K. Mäder, H.M. Swartz, Noninvasive measurement of the pH inside the gut by using pH-sensitive nitroxides. An *in vivo* EPR study, Magn. Reson. Med. 36 (1996) 694–697.

[32] M.A. Foster, I.A. Grigor'ev, D.J. Lurie, V.V. Khramtsov, S. McCallum, I. Panagiotelis, J.M. Hutchison, A. Koptioug, I. Nicholson, *In vivo* detection of a pH-sensitive nitroxide in the rat stomach by low-field ESR-based techniques, Magn. Reson. Med. 49 (2003) 558–567.

[33] J.M.S. Hutchison, A simple low-field ESR spectrometer, in: International Workshop on In Vivo EPR and Related Studies, Dartmouth Medical School, Hanover, 1998, p. 35.

[34] G. Breit, I.I. Rabi, Measurement of nuclear spin, Phys. Rev. 38 (1931) 2082–2083.

[35] I. Nicholson, F.J. Robb, D.J. Lurie, Imaging paramagnetic species using radiofrequency longitudinally detected ESR (LODESR imaging), J. Magn. Reson. Ser. B 104 (1994) 284–288.

[36] D.J. Lurie, M.A. Foster, D. Yeung, J.M. Hutchison, Design, construction and use of a large-sample field-cycled PEDRI imager, Phys. Med. Biol. 43 (1998) 1877–1886.

[37] D.J. Lurie, I. Nicholson, J.R. Mallard, Low-field EPR measurements by field-cycled dynamic nuclear polarisation, J. Magn. Res. 95 (1991) 405–409.

[38] R.J. Simpson, T.J. Peters, Forms of soluble iron in mouse stomach and duodenal lumen: significance for mucosal uptake, Br. J. Nutr. 63 (1990) 79–89.